

Towards a universal description of hadronic phase of QCD

Aman Abhishek^{1,*} and Sayantan Sharma^{1,†}

¹*The Institute of Mathematical Sciences, a CI of Homi Bhabha National Institute, Chennai, 600113, India*

Mean-field model quantum field theories of hadrons were traditionally developed to describe cold and dense nuclear matter and are by now very well constrained from the recent neutron star merger observations. We show that when augmented with additional known hadrons and resonances but not included earlier, these mean-field models can be extended beyond its regime of applicability. Calculating some specific ratios of baryon number susceptibilities for finite temperature and moderate values of baryon densities within mean-field approximation, we show that these match consistently with the lattice QCD data available at lower densities, unlike the results obtained from a non-interacting hadron resonance gas model. We also estimate the curvature of the line of constant energy density, fixed at its corresponding value at the chiral crossover transition in QCD, in the temperature-density plane. The number density at low temperatures and high density is found to be about twice the nuclear saturation density along the line of constant energy density of $\epsilon = 348 \pm 41$ MeV/fm³. Moreover from this line we can indirectly constrain the critical end-point of QCD to be beyond $\mu_B = 596$ MeV for temperature ~ 125 MeV.

PACS numbers:

Introduction Developing an effective field theory description of hadrons preceded the discovery of the field theory of strong interactions, Quantum Chromodynamics (QCD). Indeed, based on the observation of the exponential increase in the density of states of hadrons with increasing temperature, it was proposed that hadronic matter will undergo a phase transition to a deconfined phase [1]. Ab-initio lattice studies have confirmed this scenario and showed the existence of a smooth crossover at zero baryon density [2–6] from a hadron phase to a quark-gluon plasma phase in 2+1 flavor QCD with physical quark masses at a temperature $T_c = 156.5 \pm 1.5$ MeV [7]. Furthermore lattice QCD techniques have now provided us with the state-of-the art Equation of State (EoS) of hadrons in the continuum limit [8–10]. Such reliable results have boosted the efforts for understanding the different hadron interactions and develop effective relativistic quantum field theories of hadrons, the so-called *hadrodynamics*. Constraining *hadrodynamics* to a very good extent is of fundamental importance in understanding QCD at finite temperature and density.

A description of the hadron phase in terms of a gas of non-interacting hadrons and the narrow-width resonances (HRG) [11–13] has been shown to describe bulk thermodynamic observables in QCD, e.g. free-energy [14–16] and chiral condensate [17, 18] to a surprisingly good accuracy. This description is the basis for statistical hadronization models that have been very successful in describing the experimental yields of different hadron species in heavy-ion colliders [19]. A justification of this comparison came from the observation that non-resonant part of the phase shifts of the attractive hadron interactions largely cancel out in the calculation of free-energy, and the interacting part of the pressure can be well described by the contribution of resonances treated as stable particles [20]. However with increasing

precision of the lattice data on fluctuations of conserved numbers like baryon number, strangeness and electric charge, a visible departure from the HRG model predictions are by now clearly evident. Extension of the basic HRG model by augmenting it with the many not-yet experimentally measured baryon resonances [21] mainly in the strangeness sector [22], but predicted from lattice QCD and different relativistic quark models, termed as QMHRG can explain many puzzles like simultaneous freezeout of light, strange and open-charm hadrons [23–25]. However there are thermodynamic observables in QCD which cannot be yet explained within the QMHRG model, specially close to T_c [19, 26, 27], highlighting the importance of non-resonant and repulsive interaction channels.

Repulsive interactions between baryons will become more important at large baryon densities. However constraining them is challenging [28] as there are no first principles calculations of the EoS available yet from lattice QCD due to the infamous *sign-problem* [29, 30]. Experimental constraints are also few and come mainly from the study of supernovae, neutron star mergers and nuclear matter from the low energy heavy-ion collision experiments at CERN SPS and HADES, Darmstadt and in future from the upcoming FAIR facility at GSI Darmstadt and NICA at Dubna. Recent advances in the multi-messenger astronomy of neutron stars have opened a new avenue to constrain the nuclear models and its EoS [28, 31, 32]. In this regime of high baryon densities there are a multitude of nuclear models with different EoS. These are usually based on the Dirac-Brueckner-Hartree-Fock [33–35] approach or relativistic mean field models [36–38]. In the former approach parameters of the interactions are fixed from experimental inputs of nucleon-nucleon and nucleon-meson scatterings. However its application to finite density nuclear matter re-

mains difficult. On the other hand in relativistic hadron models, pioneered by Walecka, the interactions between the nucleons are implemented at mean-field level by coupling to effective meson degrees of freedom. The parameters of the interaction terms are instead determined by matching to the empirical saturation properties of nuclear matter. Recent observation of a medium sized neutron star heavier than twice the solar mass [39–42], simultaneous mass radius measurements [43–47] and bounds on tidal deformability [48, 49] during neutron star mergers have lead to more stringent constraints on the nuclear EoS [50–61] and hence on these mean-field models.

In this Letter we address the question of how well these nuclear models which are traditionally designed to explain cold-dense nuclear matter, can describe QCD thermodynamics at a relatively higher temperatures and moderate baryon densities. By extending the study of relativistic hadron models (which are well constrained from neutron-star merger observations) to moderate values of baryon densities and higher temperatures i.e. in the region $\mu_B/T = 3-5$, we estimate the hadronic freeze-out line. Using the information about the pseudo-critical line at small baryon densities from lattice QCD, we constrain the location of the critical end-point (CEP) at $\mu_{\text{CEP}}/T_{\text{CEP}} > 5$ if $T_{\text{CEP}} \sim 0.8 T_c$ [62]. The broad outline of the Letter is as follows: we begin in the next section by introducing the specific relativistic mean-field hadron model used in this work. In the subsequent sections we calculate different thermodynamic observables within these mean-field models and compare to the lattice QCD results on thermodynamic susceptibilities at finite temperatures and moderate values of net-baryon densities. We show that these mean-field models can be very well extended beyond its traditional regime of application and in some cases can explain lattice data better than QMHRG. This has deeper implications and suggest that non-resonant interactions between the hadrons are crucial to explain the lattice QCD data at moderate baryon densities revealing the universal nature of hadronic interactions.

Relativistic mean-field models for hadrodynamics : In order to choose a suitable starting point we consider a relativistic mean-field effective model which includes strange baryons [63]. This specific model along with other two models [64, 65] are very well constrained out of many hadronic models using the latest gravitational wave data coming from neutron star mergers and experimental data on nuclear skin thickness [54]. Indeed the recent ab-initio result for the neutron skin of Pb^{208} [66] is consistent with this model. The Lagrangian of this effective model [63] is explicitly discussed in Appendix I. We henceforth refer to this as model 1. In this model, the nucleon fields are coupled non-linearly to the Lorentz scalars σ, δ and vectors ρ, ω mesons. The interactions mediated by δ -mesons contribute to the asymmetry energy between protons and neutrons and is important

for the stability of the nuclei drip line. One has additionally the hyperon interactions built in it. The strength of hyperon interactions are constrained from different sources. Whereas the coupling of hyperons to vector and iso-vector mesons both with and without strangeness are constrained from $SU(6)$ symmetry within the quark model, their coupling to scalar mesons are constrained by reproducing the hyper-nuclear potentials in saturated nuclear matter.

At the mean field level, the contribution from the ω -condensate is essentially proportional to the baryon density and that from the mean σ field depends on the sum of baryon and anti-baryon densities, see Appendix II. Hence the effect of repulsive ω interactions in thermodynamic observables are visible only at finite net-baryon density, within this approximation. We will henceforth show our results at finite μ_B for two cases, i) $n_Q/n_B = 0.4$, $n_S = 0$, the so-called strangeness neutral conditions that are realized in a typical heavy-ion collision for the phase diagram and ii) $\mu_Q = 0, \mu_S = 0$ where most lattice QCD data of correlations and fluctuations of baryon number, strangeness, etc are available for comparison. In these models the mean field values of meson fields at different temperature and densities are obtained by solving a set of self-consistent equations corresponding to the nucleon masses and energies, the details of which are discussed in Appendix I. The mean fields of the different mesons which mediate interactions between baryons in model 1 are shown in Fig. 6. It is evident that the mean-values of the σ field are most sensitive to μ_B followed by the ω field. Hence for $\mu_B < 300$ MeV, the attractive interactions due to σ dominates over the repulsive vector interactions due to ω mesons. Since the strange mesons are massive, their mean-fields have a negligibly small dependence on μ_B .

How can mean-field models be extended to explain QCD thermodynamics in T - μ_B plane :

As mentioned earlier, the mean-field models were traditionally introduced to explain the nuclear liquid-gas transition in the $T \sim 0$ and large μ_B regime. We suggest here how we can extend the applicability of such models in the finite temperature and moderately high baryon number densities. We first study the ratio $\chi_{31}^{BS}/\chi_{11}^{BS}$ where we motivate the need to include additional baryons in the spectrum with suitably tuned couplings and in addition non-interacting mesons.

We show the ratio $\chi_{31}^{BS}/\chi_{11}^{BS}$ as a function of μ_B at $T = 135$ MeV and $\mu_Q = \mu_S = 0$ in Fig. 1 for $\mu_B > 400$ MeV. The lowest value of μ_B was chosen in order to have significant effect of repulsive interactions to this observable while the upper limit of μ_B is chosen such that the energy density at $T = 135$ MeV is close to $\epsilon = 348 \pm 41$ MeV/fm³. The green band represents the results from lattice QCD [67] which is extrapolated upto $\mu_B = 400$ MeV. Results from QMHRG model and model 1 are also shown in the same plot from $\mu_B = 400$ MeV to $\mu_B = 600$ MeV as solid lines in the right hand corner. The results

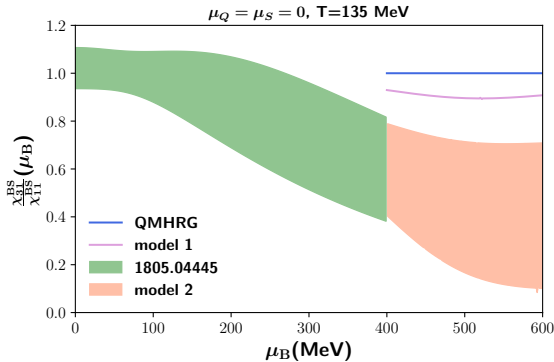


FIG. 1: The $\chi_{31}^{BS}/\chi_{11}^{BS}$ compared between lattice QCD (green band), QMHRG model (blue), model 1 (magenta) and model 2 (orange band). For model 2 the band corresponds to α varying from 0.15 to 0.2 and α_S varying from 0.15 to 0.7.

from model 1, are significantly different from QMHRG model results and is $\sim 12\%$ higher than the upper band of the lattice QCD result at $\mu_B = 400$ MeV. Thus while the inclusion of interactions which are inbuilt in model 1 improves the approach towards explaining the lattice data, clearly the presence of just two strange baryons is not enough.

This discrepancy motivates the need for extending the model 1 by including more baryons. Adding more baryons to model 1 requires the knowledge of the couplings of these additional degrees of freedom to the meson fields. These couplings cannot be fixed from experiments as not enough data is available. Another alternative is to use group theoretical arguments to relate the couplings of heavier baryons to those baryons whose couplings are known. To simplify our calculation, we instead fix the couplings of these extra baryons in a way such that couplings of non-strange degrees of freedom are taken to be a fraction of nucleon couplings and strange baryons to be a fraction of Λ -hyperon couplings. This can be mathematically written in a compact form as $g^{B-M} = \alpha g^{N-M}$ and $g^{SB-M} = \alpha_S g^{\Lambda-M}$, where B and SB denote non-strange and strange baryons respectively which are not present in model 1 but included from the QMHRG list. The N represents nucleon and M denotes mesons. The coefficients α and α_S are obtained by fitting model 2 results of $\chi_{31}^{BS}/\chi_{11}^{BS}$ to the continuum extrapolated band from lattice QCD. The model 2 results match with the upper boundary of lattice QCD data for $\alpha = \alpha_S = 0.15$. To also match the model 2 results to the lower boundary of the lattice QCD data, we have to choose $\alpha = 0.2$ and $\alpha_S = 0.7$. Thus between the upper and lower edges of the lattice data in Fig. 1, the non-strange baryon couplings change little while the strange baryon couplings vary significantly.

Now having fixed the couplings, we show what are its implications for other thermodynamic observables. In

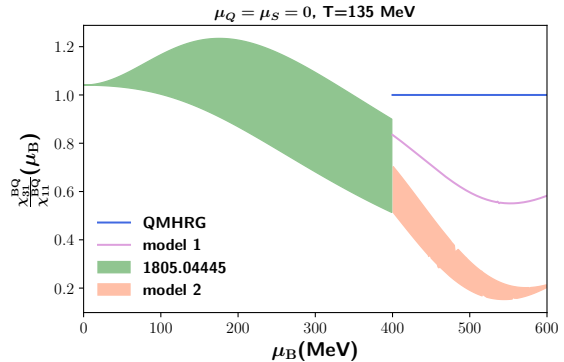


FIG. 2: The $\chi_{31}^{BQ}/\chi_{11}^{BQ}$ compared between lattice QCD (green band), QMHRG model (blue), model 1 (magenta) and model 2 (orange band).

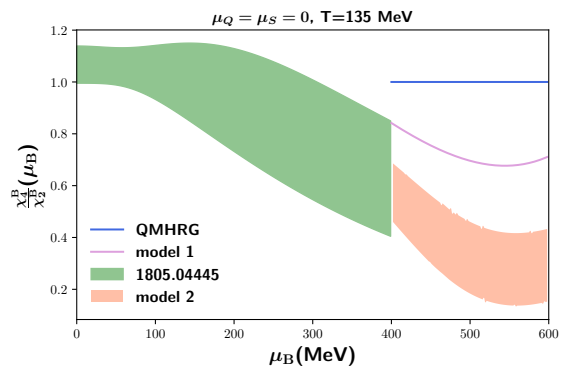


FIG. 3: The χ_4^B/χ_2^B compared between lattice QCD (green band), QMHRG model (blue), model 1 (magenta) and model 2 (orange band).

Fig. 2 we show the results for $\chi_{31}^{BQ}/\chi_{11}^{BQ}$ within model 2. Comparing with the lattice QCD results we find that the results from model 1 already agree with the lattice band but towards its upper edge. Now calculating the same observable in the model 2 with additional hadrons, we find an agreement with the lattice QCD results within a more constrained region with the lower boundaries of these bands agreeing well at $\mu_B = 400$ MeV. We recall here that the spread in model 2 results comes from the variation of α from 0.15 to 0.2 and α_S from 0.15 to 0.7.

We next show the results of another interesting observable χ_4^B/χ_2^B as a function of μ_B at $T = 135$ MeV and $\mu_Q = \mu_S = 0$. Again, the calculations within the model 1 agrees with the upper boundary of lattice band. Using model 2, we find that the results of this ratio has a smaller spread which arise due to the uncertainty in the values of the heavier baryon-meson couplings, compared to the current error band in the lattice QCD data.

Do extended mean-field models satisfy high density constraints?

Since the model 1 satisfies very well the constraints

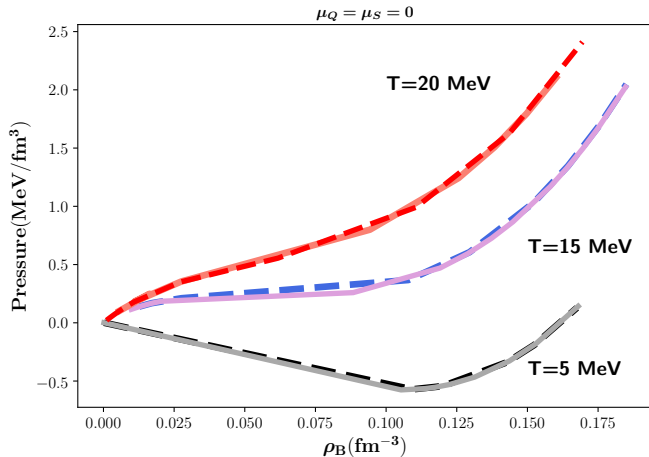


FIG. 4: Pressure as a function of baryon number density calculated from model 1 (dashed lines) and 2 (solid lines) for three different temperatures. The $T \sim 15$ MeV corresponds to nuclear liquid gas transition.

from high density matter, like nuclear liquid-gas transition, neutron star EoS, etc, we will check whether augmenting this model with additional hadrons would in anyway affect this agreement. While the contribution of heavier baryons at high densities and low temperatures are expected to be suppressed due to the thermodynamic distribution functions, their multiplicities are large which could influence the thermodynamics despite suppression of thermal distributions. To check how much of an impact these additional baryons will make, we calculate the pressure as a function of baryon densities within model 1 and model 2 for three different temperatures $T = 5, 15, 20$ MeV respectively. The ratios of couplings used for model 2 calculations have been chosen to be $\alpha = 0.2$ and $\alpha_S = 0.7$. The results of our calculation are shown in Fig. 4 as solid lines for model 2 which is compared with the dashed lines in the same plot for the model 1. As clearly seen from the plot, extending the model with the additional hadrons from QMHRG model with a large spread in the allowed values of couplings does not affect the pressure vs density curves. This gives us a proof of principle that extending mean-field nuclear models with additional baryons to explain QCD thermodynamics at high temperatures and intermediate densities will not affect its already excellent agreement at high densities and low temperatures. Our approach indeed hints to a method towards formulating a universal theory describing the hadronic phase of QCD.

Implications for the phase diagram of QCD :

Having discussed the susceptibilities in the mean-field nuclear model and its extended version, we study what insights it can give us about the phase diagram of QCD. Nuclear mean-field models do not have the $U_L(2) \times U_R(2)$ chiral symmetries in-built like the Nambu-Jona-Lasinio

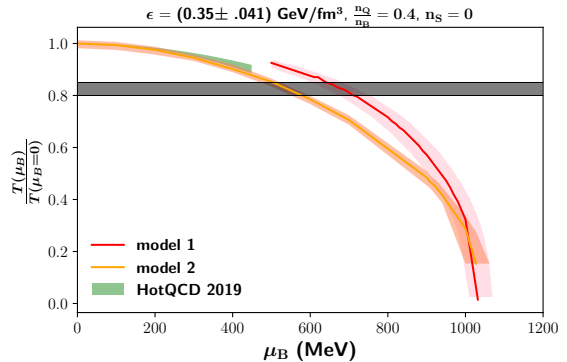


FIG. 5: Lines of constant energy density for model 1 shown as a red band and model 2 shown as an orange band. These results are compared with the chiral crossover line obtained from lattice QCD [62] and shown as a green band.

model and hence cannot describe its restoration. We thus determine the line of constant energy density in the T - μ_B plane for these models by setting $\epsilon = 348 \pm 41$ MeV/fm³ [62] which is the energy density of 2 + 1 flavor QCD at the crossover region for $\mu_B = 0$ MeV. Unlike in traditional QMHRG model, recent lattice studies have observed that the energy density along the chiral crossover line does not vary with increasing μ_B at least around $\mu_B/T \lesssim 3$ [68]. Incidentally the line of chemical freezeout of hadrons is also defined at a constant energy density [69, 70] and it approaches the chiral crossover transition line as one goes to smaller values of μ_B . The results of our calculations of lines of constant energy density in model 1 and 2 are shown in Fig. 5. These can be visualized as a chemical freezeout lines for the hadrons present within the model. Indeed the line of constant energy density in model 2 is consistent with the latest continuum extrapolated lattice QCD data, all the way from $\mu_B = 0$ MeV (extrapolated) to about $\mu_B = 450$ MeV. There is a small difference between these two results which can be accounted for from the fact that the repulsive interactions present in model 1 and 2 are insignificant at lower values of μ_B . Since the model 2 has more degrees of freedom, its line of constant energy density deviates from the model 1 calculation for $\mu_B < 900$ MeV. At higher values of μ_B , the contributions of the heavier baryons and mesons to the energy density gets suppressed due to their mass and due to lowering of temperature respectively, hence the lines of constant energy between model 1 and its extended version start to agree. Another prominent feature of the QCD phase diagram is the anticipated critical end-point (CEP) of the line of first order transitions. From the constraint that the CEP will exist in the real- μ_B plane, and its location gives the radius of convergence of thermodynamic observables, all orders of baryon number fluctuations have to be positive. Using this constraint from the lattice QCD data upto 8-

th order baryon number fluctuations at $\mu_B = 0$ [62], it is now known that $T_{\text{CEP}}/T_c < 0.85$. Noting this constraint by choosing the ratio $T/T(\mu_B = 0) = 0.8$ within the model 2 we can conclude that the CEP, if present will be at $\mu_B > 596$ MeV which provides a lower bound $\mu_B/T \sim 4.76$.

Next we calculate the curvature of these constant energy lines by fitting to the ansatz $\frac{T(\mu_B)}{T_c} = 1 - \kappa_2 \frac{\mu_B^2}{T_c^2} - \kappa_4 \frac{\mu_B^4}{T_c^4} - \kappa_6 \frac{\mu_B^6}{T_c^6}$. For model 1, the extracted curvature coefficients are $\kappa_2 = 0.020(2)$, $\kappa_4 = -0.0010(3)$, $\kappa_6 = 0.000060(3)$ which are also consistent with those calculated from model 2, $\kappa_2 = 0.020(2)$, $\kappa_4 = -0.0005(1)$ and $\kappa_6 = 0.000010(2)$. The values of κ_2 are somewhat larger than the latest continuum extrapolated lattice results of the κ_2 [62, 71, 72] extracted from the renormalized chiral condensate and from a recent HRG model estimate [18], which is expected as the results from these models are for the entire T - μ_B plane. The value of κ_4 from lattice QCD is consistent with zero [62, 72], whereas we find a negative but finite value in both the models. The results for κ_6 are new and it is about 1000 times smaller than κ_2 . Thus its effect should start become significant at $\mu_B/T \sim 15$, well within the cold nuclear matter regime. Moreover the baryon densities obtained in model 1 and 2 for a typical neutron star environment characterized with $n_Q/n_B = 0.05$ - 0.2 , $n_S = 0$, varies from 0.28 fm^{-3} to 0.35 fm^{-3} as energy density varies from $\epsilon = 307$ - 389 MeV/fm^3 . The variation in the ratio for n_Q/n_B has a tiny effect on this density. It is remarkable that the typical nuclear densities we obtain from these models are about twice the nuclear saturation density, when many-body interactions start to become dominant [73] and quark exchanges are expected to mediate baryon interactions [74]. Our calculations also support this picture albeit indirectly that a mixed phase of quarks and hadrons can survive in neutron star cores with baryon densities greater than 0.35 fm^{-3} .

Implications of lattice QCD data at $\mu_B = 0$ for high density models : Comparisons of lattice QCD data with QMHRG model particularly for observables like χ_4^B/χ_2^B [26] and higher order baryon number susceptibilities [16] clearly highlight the importance of including repulsive interactions within the QMHRG model. In our present study of nuclear model quantum field theories, the repulsive interactions at low baryon densities are negligible at the mean-field level. Unless there is a mechanism by which sufficient strength of repulsive interactions are generated at low baryon densities by calculating beyond mean-field effects, it would then imply that these models require suitable modifications to account for such interactions. In this way one can achieve a universal hadronic model, which is valid for both lower as well as high baryon densities. Furthermore our comparison of quantities like $\chi_{31}^{BS}/\chi_{11}^{BS}$ with the lattice data to extract the baryon-meson couplings in the model 2,

will benefit from an increasing precision of the lattice QCD data. This will allow for a tighter constraint on the values of the couplings of strange baryons with mesons.

Conclusions : We started this work with a question of how well the traditional nuclear mean-field models, developed for the understanding of physics at low temperatures and large baryon densities can be used to explain QCD thermodynamics at high temperatures and moderate densities. A remarkable observation that comes out of our study is that augmenting these simple models with a complete list of baryons present in QMHRG model and tuning the couplings of their interactions with mesons through a comparison with lattice QCD data of a particular observable, leads to a very good description of QCD thermodynamics at intermediate densities. In our investigation we have found that the simple baryon-meson interactions built within the nuclear models are important in bridging the gap between lattice and other non-interacting hadron models like QMHRG. Furthermore we have shown that the inclusion of these additional hadrons do not affect the nuclear liquid-gas transition, which is well-studied in the original versions of these mean-field models.

This allows for a route to identify the relevant baryon interactions in chiral symmetry broken phase, which indeed if accounted for correctly will be valid for the entire regime of densities and temperatures. However at present there are not much data available, either from experiments or theory in constraining most of these baryon-meson couplings. Our method for determining these couplings from comparison with a particular thermodynamic observable from lattice, is one such possibility since in this process the benchmark data comes from the fundamental theory of strong interactions i.e., QCD. We highlighted the need of high-precision lattice data which will allow for constraining such couplings further. This will allow for a better synergy between lattice QCD and such model quantum field theory calculations in future.

There are several directions still remaining to be explored. Firstly it would be interesting to extend this study beyond the mean-field approximation and check whether it can account for the repulsive interactions that exist among baryons and mesons, even at low densities and high temperatures, evident from comparisons of lattice QCD data with QMHRG. Another aspect towards building a universal hadronic model requires high density nuclear models to incorporate spontaneous chiral symmetry breaking. This can be achieved by including parity doublet partners like the pion degrees of freedom and the critical σ -modes, important for understanding the nature of the chiral phase transition at high densities and the thermodynamics near the critical end-point.

Acknowledgements : S.S. gratefully acknowledges support from the Department of Science and Technology, Government of India through a Ramanujan Fellowship. We would like to thank Deeptak Biswas, Jishnu

Goswami, Hiranmaya Mishra and Jan Pawłowski for helpful discussions and correspondence.

Appendix I: Details of the numerical calculations with Model 1

The Lagrangian describing model 1 [63] is given as :

$$\begin{aligned}
\mathcal{L} = & \bar{\psi} [\gamma_\mu (i\partial^\mu - g_\omega \omega^\mu - g_\rho \rho^\mu \tau - g_{\phi B} \phi^\mu) \\
& - (M - g_\sigma \sigma - g_\delta \delta \tau - g_{\sigma^* B} \sigma^*)] \psi \\
& + \frac{1}{2} (\partial_\mu \sigma \partial^\mu \sigma - m_\sigma^2 \sigma^2) - \frac{1}{3} b_\sigma M (g_\sigma \sigma)^3 - \frac{1}{4} c_\sigma (g_\sigma \sigma)^4 \\
& - \frac{1}{4} (\omega_{\mu\nu} \omega^{\mu\nu}) + \frac{1}{2} m_\omega^2 (\omega_\mu \omega^\mu) + \frac{1}{4} c_\omega (g_\omega^2 \omega_\mu \omega^\mu)^2 \\
& + \frac{1}{2} (\partial_\mu \delta \partial^\mu \delta - m_\delta^2 \delta^2) + \frac{1}{2} m_\rho^2 \rho^\mu \cdot \rho_\mu - \frac{1}{4} (\rho_{\mu\nu} \rho^{\mu\nu}) \\
& + \frac{1}{2} \Lambda_V (g_\rho^2 \rho_\mu \cdot \rho^\mu) (g_\omega^2 \omega_\mu \omega^\mu) + \frac{1}{2} (\partial_\mu \sigma^* \partial^\mu \sigma^* - m_{\sigma^*}^2 \sigma^{*2}) \\
& + \frac{1}{2} m_\phi^2 \phi_\mu \phi^\mu - \frac{1}{4} \phi_{\mu\nu} \phi^{\mu\nu} \\
& + \sum_{e,\mu} \bar{\psi}_{e,\mu} (i\gamma_\mu \partial^\mu - m_{e,\mu}) \psi_{e,\mu}.
\end{aligned}$$

Using this Lagrangian we have derived the equation of motion for the meson fields in the mean-field approximation. In this approximation the meson fields are approximated by the spacetime independent values satisfying the equations of motion and constraints for the net-electric charge and strangeness densities. The mean field equations which we solve are,

$$m_\sigma^2 \sigma = g_\sigma \left[\sum_B \frac{g_{\sigma B}}{g_\sigma} \rho_B^S - b_\sigma M (g_\sigma \sigma)^2 - c_\sigma (g_\sigma)^3 \right]$$

$$m_\omega^2 \omega^\nu = g_\omega \left[\sum_B \frac{g_{\omega B}}{g_\omega} \rho_B^B - c_\omega M (\omega_\mu \omega^\mu \omega_\mu) - g_\rho^2 \rho_\mu \cdot \rho^\mu \Lambda_V g_\omega \omega_\mu \right]$$

$$m_\rho^2 \rho^\nu = g_\rho \left[\sum_B \frac{g_{\rho B}}{g_\rho} \rho_B^B \tau - g_\rho \rho_\mu \Lambda_V g_\omega^2 \omega_\mu \omega^\mu \right]$$

$$m_\delta^2 \delta = g_\delta \sum_B \frac{g_{\delta B}}{g_\delta} \rho_B^S \tau$$

$$m_{\sigma^*}^2 \delta = g_{\sigma^* \Lambda} \sum_B \frac{g_{\sigma^* B}}{g_{\sigma^* \Lambda}} \rho_B^S$$

$$m_\phi^2 \phi^\nu = g_{\phi \Lambda} \sum_B \frac{g_{\phi B}}{g_{\phi \Lambda}} \rho_B^B.$$

The values of the different couplings and other details can be found in Ref. [63]. Once the values of mean fields

are known from the solutions of these equations satisfying the constraints, the pressure can be calculated. The susceptibilities can then be calculated by taking the derivatives of pressure with respect to different chemical potentials corresponding to baryon number, strangeness, etc. We schematically show our calculation in the following equations where X_i are the mean fields, μ_j denote the chemical potentials and \vec{f} denote the gap equations obtained from equations of motion and \vec{g} are the constraints on the system.

$$P(X_i, \mu_j, T) = 0, \quad (1)$$

$$\vec{f}(X_i, \mu_j, T) = 0, \quad (2)$$

$$\vec{g}(X_i, \mu_j, T) = 0. \quad (3)$$

To calculate the derivatives one can use the finite difference method which is numerically accurate upto $\mathcal{O}(\delta\mu_k)$. Moreover the truncation error increases with increasing order of the derivatives. We thus follow a different procedure. Instead of differentiating numerically, we use the gap and constraint equations to calculate the derivatives analytically. This is possible because these equations are satisfied at each values of T and μ_k , and the total derivative of each of them is zero.

$$\frac{\partial \vec{f}}{\partial \mu_k} + \frac{\partial \vec{f}}{\partial X_i} \frac{dX_i}{d\mu_k} + \frac{\partial \vec{f}}{\partial \mu_j} \frac{d\mu_j}{d\mu_k} = 0, \quad (4)$$

$$\frac{\partial \vec{g}}{\partial \mu_k} + \frac{\partial \vec{g}}{\partial X_i} \frac{dX_i}{d\mu_k} + \frac{\partial \vec{g}}{\partial \mu_j} \frac{d\mu_j}{d\mu_k} = 0. \quad (5)$$

These are linear equations in the derivatives $\frac{dX_i}{d\mu_k}$ and $\frac{d\mu_j}{d\mu_k}$. Solving for the above equations gives the first order derivatives of mean fields. Once first order derivatives are known, these equations can be successively differentiated to find further higher order derivatives.

Appendix II : The various meanfields as a function of μ_B

In Fig. 6 we have shown σ and ω mean fields in model 1 [63] as a function of the baryon chemical potential. From the plot we observe that as μ_B increases, the mean-field values of σ and ω fields also increases, hence the interactions mediated by these mesons become more relevant. This is because the mean-field values for σ and ω fields are proportional to scalar and baryon densities respectively, which increase with the baryon chemical potential. The ρ and δ mean-fields are proportional to the isospin baryon and scalar densities respectively. Since the isospin chemical potential is negligibly small, these mean-fields remain insignificant. The σ_s and ϕ_s mesons couple only to strange baryons which are heavy and thus their mean-field values remain small. The mean-fields which

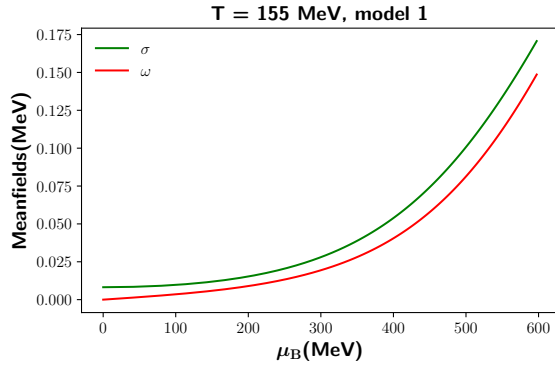


FIG. 6: The σ and ω mean-field value as a function of μ_B for $T = 155$ MeV. Other mean-fields are much smaller.

increase the pressure correspond to mesons which mediate repulsive interactions and which decreases the value of pressure correspond to attractive interactions. The ω thus mediates repulsive interactions and the σ mediates attractive interactions. One may note that while fields other than σ and ω are small and not shown in Fig. 6, they play an important role at high density and low temperature in fitting the experimental data.

* Electronic address: amanabhi@imsc.res.in

† Electronic address: sayantans@imsc.res.in

- [1] R. Hagedorn, “Statistical thermodynamics of strong interactions at high-energies,” *Nuovo Cim. Suppl.*, vol. 3, pp. 147–186, 1965.
- [2] Y. Aoki, G. Endrodi, Z. Fodor, S. D. Katz, and K. K. Szabo, “The Order of the quantum chromodynamics transition predicted by the standard model of particle physics,” *Nature*, vol. 443, pp. 675–678, 2006.
- [3] A. Bazavov *et al.*, “The chiral and deconfinement aspects of the QCD transition,” *Phys. Rev. D*, vol. 85, p. 054503, 2012.
- [4] T. Bhattacharya *et al.*, “QCD Phase Transition with Chiral Quarks and Physical Quark Masses,” *Phys. Rev. Lett.*, vol. 113, no. 8, p. 082001, 2014.
- [5] F. Burger, E.-M. Ilgenfritz, M. P. Lombardo, and A. Trunin, “Chiral observables and topology in hot QCD with two families of quarks,” *Phys. Rev. D*, vol. 98, no. 9, p. 094501, 2018.
- [6] Y. Taniguchi, S. Ejiri, K. Kanaya, M. Kitazawa, H. Suzuki, and T. Umeda, “ $N_f = 2+1$ QCD thermodynamics with gradient flow using two-loop matching coefficients,” *Phys. Rev. D*, vol. 102, no. 1, p. 014510, 2020. [Erratum: *Phys.Rev.D* 102, 059903 (2020)].
- [7] A. Bazavov *et al.*, “Chiral crossover in QCD at zero and non-zero chemical potentials,” *Phys. Lett. B*, vol. 795, pp. 15–21, 2019.
- [8] S. Borsanyi, Z. Fodor, C. Hoelbling, S. D. Katz, S. Krieg, and K. K. Szabo, “Full result for the QCD equation of state with 2+1 flavors,” *Phys. Lett. B*, vol. 730, pp. 99–104, 2014.
- [9] A. Bazavov *et al.*, “Equation of state in (2+1)-flavor QCD,” *Phys. Rev. D*, vol. 90, p. 094503, 2014.
- [10] H. T. Ding, S. Mukherjee, H. Ohno, P. Petreczky, and H. P. Schadler, “Diagonal and off-diagonal quark number susceptibilities at high temperatures,” *Phys. Rev. D*, vol. 92, no. 7, p. 074043, 2015.
- [11] R. Dashen, S.-K. Ma, and H. J. Bernstein, “S Matrix formulation of statistical mechanics,” *Phys. Rev.*, vol. 187, pp. 345–370, 1969.
- [12] R. F. Dashen and R. Rajaraman, “Narrow Resonances in Statistical Mechanics,” *Phys. Rev. D*, vol. 10, p. 694, 1974.
- [13] R. F. Dashen and R. Rajaraman, “Effective Elementarity of Resonances and Bound States in Statistical Mechanics,” *Phys. Rev. D*, vol. 10, p. 708, 1974.
- [14] F. Karsch, K. Redlich, and A. Tawfik, “Hadron resonance mass spectrum and lattice QCD thermodynamics,” *Eur. Phys. J. C*, vol. 29, pp. 549–556, 2003.
- [15] F. Karsch, K. Redlich, and A. Tawfik, “Thermodynamics at nonzero baryon number density: A Comparison of lattice and hadron resonance gas model calculations,” *Phys. Lett. B*, vol. 571, pp. 67–74, 2003.
- [16] P. Huovinen and P. Petreczky, “QCD Equation of State and Hadron Resonance Gas,” *Nucl. Phys. A*, vol. 837, pp. 26–53, 2010.
- [17] S. Borsanyi, Z. Fodor, C. Hoelbling, S. D. Katz, S. Krieg, C. Ratti, and K. K. Szabo, “Is there still any T_c mystery in lattice QCD? Results with physical masses in the continuum limit III,” *JHEP*, vol. 09, p. 073, 2010.
- [18] D. Biswas, P. Petreczky, and S. Sharma, “Chiral condensate from a hadron resonance gas model,” *Phys. Rev. C*, vol. 106, no. 4, p. 045203, 2022.
- [19] A. Andronic, P. Braun-Munzinger, K. Redlich, and J. Stachel, “Decoding the phase structure of QCD via particle production at high energy,” *Nature*, vol. 561, no. 7723, pp. 321–330, 2018.
- [20] R. Venugopalan and M. Prakash, “Thermal properties of interacting hadrons,” *Nucl. Phys. A*, vol. 546, pp. 718–760, 1992.
- [21] A. Majumder and B. Muller, “Hadron Mass Spectrum from Lattice QCD,” *Phys. Rev. Lett.*, vol. 105, p. 252002, 2010.
- [22] A. Bazavov *et al.*, “Strangeness at high temperatures: from hadrons to quarks,” *Phys. Rev. Lett.*, vol. 111, p. 082301, 2013.
- [23] A. Bazavov *et al.*, “Additional Strange Hadrons from QCD Thermodynamics and Strangeness Freezeout in Heavy Ion Collisions,” *Phys. Rev. Lett.*, vol. 113, no. 7, p. 072001, 2014.
- [24] A. Bazavov *et al.*, “The melting and abundance of open charm hadrons,” *Phys. Lett. B*, vol. 737, pp. 210–215, 2014.
- [25] S. Mukherjee, P. Petreczky, and S. Sharma, “Charm degrees of freedom in the quark gluon plasma,” *Phys. Rev. D*, vol. 93, no. 1, p. 014502, 2016.
- [26] D. Bollweg, J. Goswami, O. Kaczmarek, F. Karsch, S. Mukherjee, P. Petreczky, C. Schmidt, and P. Scior, “Second order cumulants of conserved charge fluctuations revisited: Vanishing chemical potentials,” *Phys. Rev. D*, vol. 104, no. 7, 2021.
- [27] J. M. Karthein, V. Koch, C. Ratti, and V. Vovchenko, “Constraining the hadronic spectrum and repulsive interactions in a hadron resonance gas via fluctuations of conserved charges,” *Phys. Rev. D*, vol. 104, no. 9, p. 094009, 2021.

- 2021.
- [28] A. Lovato *et al.*, “Long Range Plan: Dense matter theory for heavy-ion collisions and neutron stars,” 11 2022.
- [29] P. de Forcrand, “Simulating QCD at finite density,” *PoS*, vol. LAT2009, p. 010, 2009.
- [30] C. Schmidt and S. Sharma, “The phase structure of QCD,” *J. Phys. G*, vol. 44, no. 10, p. 104002, 2017.
- [31] E. Annala, T. Gorda, E. Katerini, A. Kurkela, J. Nättilä, V. Paschalidis, and A. Vuorinen, “Multimessenger Constraints for Ultradense Matter,” *Phys. Rev. X*, vol. 12, no. 1, p. 011058, 2022.
- [32] K. Sumiyoshi, T. Kojo, and S. Furusawa, “Equation of state in neutron stars and supernovae,” 6 2022.
- [33] R. Brockmann and R. Machleidt, “Nuclear Saturation in a Relativistic Bruckner-Hartree-Fock Approach,” *Phys. Lett. B*, vol. 149, p. 283, 1984.
- [34] B. Ter Haar and R. Malfliet, “Nucleons, Mesons and Deltas in Nuclear Matter. A Relativistic Dirac-Bruckner Approach,” *Phys. Rept.*, vol. 149, pp. 207–286, 1987.
- [35] F. de Jong and H. Lenske, “Asymmetric nuclear matter in the relativistic Bruckner Hartree-Fock approach,” *Phys. Rev. C*, vol. 57, pp. 3099–3107, 1998.
- [36] B. D. Serot and J. D. Walecka, “The Relativistic Nuclear Many Body Problem,” *Adv. Nucl. Phys.*, vol. 16, pp. 1–327, 1986.
- [37] B. D. Serot and J. D. Walecka, “Recent progress in quantum hadrodynamics,” *Int. J. Mod. Phys. E*, vol. 6, pp. 515–631, 1997.
- [38] A. R. Bodmer, “Relativistic mean field theory of nuclei with a vector meson selfinteraction,” *Nucl. Phys. A*, vol. 526, pp. 703–721, 1991.
- [39] B. Margalit and B. D. Metzger, “Constraining the Maximum Mass of Neutron Stars From Multi-Messenger Observations of GW170817,” *Astrophys. J. Lett.*, vol. 850, no. 2, p. L19, 2017.
- [40] M. Shibata, S. Fujibayashi, K. Hotokezaka, K. Kiuchi, K. Kyutoku, Y. Sekiguchi, and M. Tanaka, “Modeling GW170817 based on numerical relativity and its implications,” *Phys. Rev. D*, vol. 96, no. 12, p. 123012, 2017.
- [41] L. Rezzolla, E. R. Most, and L. R. Weih, “Using gravitational-wave observations and quasi-universal relations to constrain the maximum mass of neutron stars,” *Astrophys. J. Lett.*, vol. 852, no. 2, p. L25, 2018.
- [42] M. Ruiz, S. L. Shapiro, and A. Tsokaros, “GW170817, General Relativistic Magnetohydrodynamic Simulations, and the Neutron Star Maximum Mass,” *Phys. Rev. D*, vol. 97, no. 2, p. 021501, 2018.
- [43] T. E. Riley *et al.*, “A *NICER* View of PSR J0030+0451: Millisecond Pulsar Parameter Estimation,” *Astrophys. J. Lett.*, vol. 887, no. 1, p. L21, 2019.
- [44] M. C. Miller *et al.*, “PSR J0030+0451 Mass and Radius from *NICER* Data and Implications for the Properties of Neutron Star Matter,” *Astrophys. J. Lett.*, vol. 887, no. 1, p. L24, 2019.
- [45] T. E. Riley *et al.*, “A *NICER* View of the Massive Pulsar PSR J0740+6620 Informed by Radio Timing and XMM-Newton Spectroscopy,” *Astrophys. J. Lett.*, vol. 918, no. 2, p. L27, 2021.
- [46] M. C. Miller *et al.*, “The Radius of PSR J0740+6620 from *NICER* and XMM-Newton Data,” *Astrophys. J. Lett.*, vol. 918, no. 2, p. L28, 2021.
- [47] E. Fonseca *et al.*, “Refined Mass and Geometric Measurements of the High-mass PSR J0740+6620,” *Astrophys. J. Lett.*, vol. 915, no. 1, p. L12, 2021.
- [48] B. P. Abbott *et al.*, “GW170817: Observation of Gravitational Waves from a Binary Neutron Star Inspiral,” *Phys. Rev. Lett.*, vol. 119, no. 16, p. 161101, 2017.
- [49] T. Hinderer, B. D. Lackey, R. N. Lang, and J. S. Read, “Tidal deformability of neutron stars with realistic equations of state and their gravitational wave signatures in binary inspiral,” *Phys. Rev. D*, vol. 81, p. 123016, 2010.
- [50] F. Douchin and P. Haensel, “A unified equation of state of dense matter and neutron star structure,” *Astron. Astrophys.*, vol. 380, p. 151, 2001.
- [51] K. Chatziioannou, K. Yagi, A. Klein, N. Cornish, and N. Yunes, “Probing the Internal Composition of Neutron Stars with Gravitational Waves,” *Phys. Rev. D*, vol. 92, no. 10, p. 104008, 2015.
- [52] E. Annala, T. Gorda, A. Kurkela, and A. Vuorinen, “Gravitational-wave constraints on the neutron-star-matter Equation of State,” *Phys. Rev. Lett.*, vol. 120, no. 17, p. 172703, 2018.
- [53] I. Tews, J. Margueron, and S. Reddy, “Critical examination of constraints on the equation of state of dense matter obtained from GW170817,” *Phys. Rev. C*, vol. 98, no. 4, p. 045804, 2018.
- [54] R. Nandi, P. Char, and S. Pal, “Constraining the relativistic mean-field model equations of state with gravitational wave observations,” *Phys. Rev. C*, vol. 99, no. 5, p. 052802, 2019.
- [55] L. McLerran and S. Reddy, “Quarkyonic Matter and Neutron Stars,” *Phys. Rev. Lett.*, vol. 122, no. 12, p. 122701, 2019.
- [56] E. Annala, T. Gorda, A. Kurkela, J. Nättilä, and A. Vuorinen, “Evidence for quark-matter cores in massive neutron stars,” *Nature Phys.*, vol. 16, no. 9, pp. 907–910, 2020.
- [57] M. M. Forbes, S. Bose, S. Reddy, D. Zhou, A. Mukherjee, and S. De, “Constraining the neutron-matter equation of state with gravitational waves,” *Phys. Rev. D*, vol. 100, no. 8, p. 083010, 2019.
- [58] G. Baym, S. Furusawa, T. Hatsuda, T. Kojo, and H. Togashi, “New Neutron Star Equation of State with Quark-Hadron Crossover,” *Astrophys. J.*, vol. 885, p. 42, 2019.
- [59] C. Drischler, S. Han, J. M. Lattimer, M. Prakash, S. Reddy, and T. Zhao, “Limiting masses and radii of neutron stars and their implications,” *Phys. Rev. C*, vol. 103, no. 4, p. 045808, 2021.
- [60] T. Kojo, D. Hou, J. Okafor, and H. Togashi, “Phenomenological QCD equations of state for neutron star dynamics: Nuclear-2SC continuity and evolving effective couplings,” *Phys. Rev. D*, vol. 104, no. 6, p. 063036, 2021.
- [61] C. Drischler, R. J. Furnstahl, J. A. Melendez, and D. R. Phillips, “How Well Do We Know the Neutron-Matter Equation of State at the Densities Inside Neutron Stars? A Bayesian Approach with Correlated Uncertainties,” *Phys. Rev. Lett.*, vol. 125, no. 20, p. 202702, 2020.
- [62] A. Bazavov *et al.*, “The QCD Equation of State to $\mathcal{O}(\mu_B^6)$ from Lattice QCD,” *Phys. Rev. D*, vol. 95, no. 5, p. 054504, 2017.
- [63] J. K. Bunta and S. Gmuca, “Hyperons in a relativistic mean-field approach to asymmetric nuclear matter,” *Phys. Rev. C*, vol. 70, p. 054309, 2004.
- [64] B. Liu, V. Greco, V. Baran, M. Colonna, and M. Di Toro, “Asymmetric nuclear matter: The Role of the isovector scalar channel,” *Phys. Rev. C*, vol. 65, p. 045201, 2002.
- [65] S. Typel and H. H. Wolter, “Relativistic mean field calculations with density dependent meson nucleon coupling,”

- Nucl. Phys. A*, vol. 656, pp. 331–364, 1999.
- [66] B. Hu *et al.*, “Ab initio predictions link the neutron skin of ^{208}Pb to nuclear forces,” *Nature Phys.*, vol. 18, no. 10, pp. 1196–1200, 2022.
- [67] S. Borsanyi, Z. Fodor, J. N. Guenther, S. K. Katz, K. K. Szabo, A. Pasztor, I. Portillo, and C. Ratti, “Higher order fluctuations and correlations of conserved charges from lattice QCD,” *JHEP*, vol. 10, p. 205, 2018.
- [68] D. Bollweg, D. A. Clarke, J. Goswami, O. Kaczmarek, F. Karsch, S. Mukherjee, P. Petreczky, C. Schmidt, and S. Sharma, “Equation of state and speed of sound of (2+1)-flavor QCD in strangeness-neutral matter at non-vanishing net baryon-number density,” 12 2022.
- [69] F. Becattini, M. Gazdzicki, and J. Sollfrank, “On chemical equilibrium in nuclear collisions,” *Eur. Phys. J. C*, vol. 5, pp. 143–153, 1998.
- [70] D. Teaney, “Chemical freezeout in heavy ion collisions,” 4 2002.
- [71] C. Bonati, M. D’Elia, F. Negro, F. Sanfilippo, and K. Zambello, “Curvature of the pseudocritical line in QCD: Taylor expansion matches analytic continuation,” *Phys. Rev. D*, vol. 98, no. 5, p. 054510, 2018.
- [72] S. Borsanyi, Z. Fodor, J. N. Guenther, R. Kara, S. D. Katz, P. Parotto, A. Pasztor, C. Ratti, and K. K. Szabo, “QCD Crossover at Finite Chemical Potential from Lattice Simulations,” *Phys. Rev. Lett.*, vol. 125, no. 5, p. 052001, 2020.
- [73] A. Akmal, V. R. Pandharipande, and D. G. Ravenhall, “The Equation of state of nucleon matter and neutron star structure,” *Phys. Rev. C*, vol. 58, pp. 1804–1828, 1998.
- [74] K. Fukushima, T. Kojo, and W. Weise, “Hard-core deconfinement and soft-surface delocalization from nuclear to quark matter,” *Phys. Rev. D*, vol. 102, no. 9, p. 096017, 2020.